Constant DC-Capacitor Voltage-Control-Based Harmonics Compensation Strategy of Smart Charger for Electric Vehicles in Single-Phase Three-Wire Distribution Feeders

Fuka Ikeda [1,†], Hiroaki Yamada [1,†], Toshihiko Tanaka [1,*,†] and Masayuki Okamoto [2,†]

[1] Department of Electrical and Electronic Engineering, Yamaguchi University, 2-16-1 Tokiwadai, Ube, Yamaguchi 755-8611, Japan; fuka@yamaguchi-u.ac.jp (F.I.); hiro-ymd@yamaguchi-u.ac.jp (H.Y.)
[2] Department of Electrical Engineering, National Institute of Technology, Ube College, 2-14-1 Tokiwadai, Ube, Yamaguchi 755-8555, Japan; mokamoto@ube-k.ac.jp
[*] Correspondence: totanaka@yamaguchi-u.ac.jp; Tel.: +81-836-85-9400
[†] These authors contributed equally to this work.

Abstract: This paper discusses harmonic current compensation of the constant DC-capacitor voltage-control (CDCVC)-based strategy of smart chargers for electric vehicles (EVs) in single-phase three-wire distribution feeders (SPTWDFs) under nonlinear load conditions. The basic principle of the CDCVC-based harmonics compensation strategy under nonlinear load conditions is discussed in detail. The instantaneous power flowing into the three-leg pulse-width modulated (PWM) rectifier, which performs as a smart charger, shows that the CDCVC-based strategy achieves balanced and sinusoidal source currents with a unity power factor. The CDCVC-based harmonics compensation strategy does not require any calculation blocks of fundamental reactive, unbalanced active, and harmonic currents. Thus, the authors propose a simplified algorithm to compensate for reactive, unbalanced active, and harmonic currents. A digital computer simulation is implemented to confirm the validity and high practicability of the CDCVC-based harmonics compensation strategy using PSIM software. Simulation results demonstrate that balanced and sinusoidal source currents with a unity power factor in SPTWDFs are obtained on the secondary side of the pole-mounted distribution transformer (PMDT) during both the battery-charging and discharging operations in EVs, compensating for the reactive, unbalanced active, and harmonic currents.

Keywords: smart charger; single-phase three-wire distribution feeders (SPTWDFs); harmonics compensation; constant DC-capacitor voltage control (CDCVC); three-leg PWM rectifier; bidirectional DC-DC converter; single-phase PLL circuit; single-phase *d-q* coordinate

1. Introduction

Smart meters are now installed for domestic consumers in areas serviced by the Tokyo Electric Power Company and the Kansai Electric Power Company, but not for commercial consumers [1]. These smart meters report the power consumption conditions of each domestic consumer to the electric power companies. It is natural that household electricity prices associated with high quality power consumption should be lower than those for the consumers with low quality power consumptions. Thus, in the near future, each domestic consumer will take responsibility for improving the quality of their power consumption. In Japan, single-phase three-wire distribution feeders (SPTWDFs) with pole-mounted distribution transformers (PMDTs) are used for domestic consumers. Figure 1 shows a circuit diagram of a typical SPTWDF with a PMDT. Consumer electronics in Japan are divided

into two categories depending on their capacity. Large-capacity consumer electronics are connected to Feeder1 and Feeder2 as Load3, and their voltage rating is 210 Vrms. Small-capacity consumer electronics are connected to each feeder with neutral lines as Load1 and Load2, and their voltage rating is 105 Vrms. Load conditions in domestic consumers are always unbalanced. These unbalanced conditions cause the unbalanced voltage on the secondary side of the PMDTs. The secondary side source currents of the PMDTs are also unbalanced. It well known that these unbalanced source–current conditions increase losses in the PMDTs. Power companies compensate for these losses although the losses are caused by domestic consumers. There are a large number of PMDTs in Japan, so that total economic losses are great. It is also natural that domestic consumers should be responsible for the loss compensation in PMDTs.
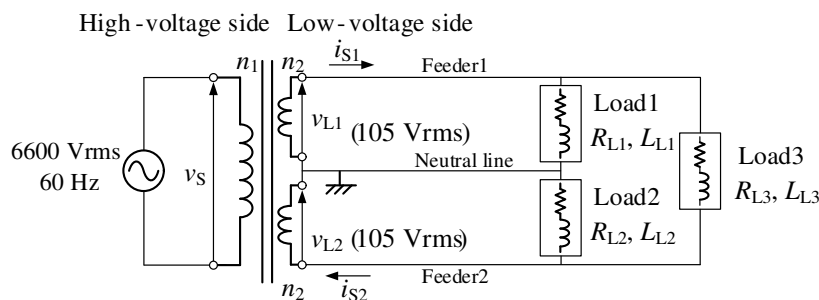

Figure 1. Typical single-phase three-wire distribution feeder (SPTWDF) used in Japan.

Electric vehicles (EVs), such as the Mitsubishi i-MiEV, a five-door hatchback kei car, and the Nissan LEAF, a medium-sized five-door hatchback car, are now commercially available in Japan. The lithium-ion batteries equipped in the i-MiEV can store 16 kWh, whereas the maximum stored power in the LEAF is 30 kWh. These EVs are highly mobile with the stored power. With this mobility, the concept of injecting power stored in EVs into the grid or home (Vehicle-to-Grid, and Vehicle-to-Home) was proposed [2–5]. A pulse-width modulated (PWM) rectifier with a bidirectional DC-DC converter was used with a photovoltaic (PV) system [6], and control and power management of the PV system were discussed. Various studies analyzing the value and potential impact on the utility grid were reported [7–9]. The analysis of the reactive power operation in a charger was described in detail. The operation modes of the proposed battery charger were divided into quadrants based on the active and reactive powers on the AC side. In addition, the control method, DC capacitor design, ac inductor design, and loss evaluation were discussed. If the charger in [7–9] is connected to SPTWDFs, perfect reactive power compensation for each feeder with a unity power factor cannot be achieved on the low-voltage side. However, unbalanced conditions remain on the secondary side of the PMDT. Balancing the currents on the two feeders is effective for balancing the feeder voltages and reducing the losses.

As described above, domestic consumers should be responsible for improving the quality of their power consumption in the near future with the smart meters, which are used to report the quality of their power consumption of each domestic consumer to the electric power companies. Thus, the present authors previously proposed a smart charger for EVs with a power quality compensator in SPTWDFs [10]. Figure 2 shows a power circuit diagram of the previously proposed smart charger for EVs with a power quality compensator [10]. The proposed smart charger consists of four-leg insulated-gate bipolar transistors (IGBTs). The first leg and second leg are connected to Feeder1 and Feeder2, respectively. The third leg is connected to the neutral line. This is an advantage of the proposed smart charger as compared to the chargers proposed in [7–9]. This PWM rectifier can compensate reactive and unbalanced active currents in SPTWDFs by canceling the neutral line current. The fourth leg is used as a bidirectional DC-DC converter for both the battery-charging and -discharging operations in EVs. The LCL filters with two capacitors effectively eliminate the switching

ripples of charger currents i_{C1}, i_{C2}, and i_{C3} because the third leg is connected to the neutral line, which is grounded. For the control strategy of the three-leg PWM rectifier in Figure 2, only a constant DC-capacitor voltage control (CDCVC), which is commonly used in active power-line conditioners, is used. This simple control algorithm achieves balanced source currents with a unity power factor. Simulation and experimental results demonstrated that balanced source currents with a unity power factor are obtained on the source side of SPTWDFs during both the battery-charging and discharging operations in EVs.
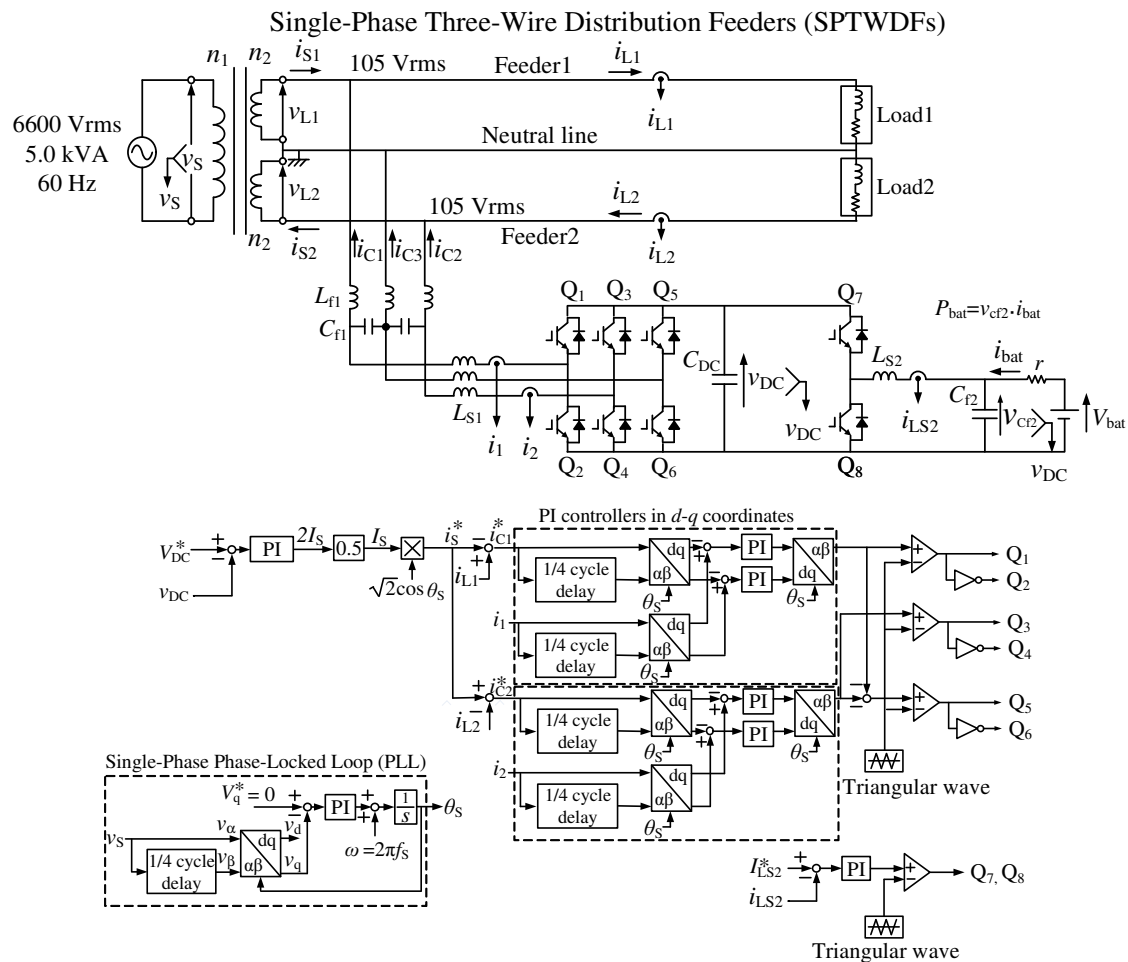

Figure 2. Power circuit diagram of the previously proposed smart charger for electric vehicles (EVs) with a power quality compensator [10].

As described before, large-capacity consumer electronics are connected to Feeder1 and Feeder2, and their voltage rating is 210 Vrms. Typical large-capacity consumer electronics are air conditioners for large rooms and induction heating (IH) cookers. Small-capacity consumer electronics are connected to each feeders with a neutral line, and their voltage rating is 105 Vrms. Typical small-capacity consumer electronics include air conditioners for small rooms, refrigerators, personal computers, liquid crystal display televisions, and illuminators. Thus, diode rectifiers are used in modern consumer electronics to convert AC voltage to DC voltage. For example, Figure 3 shows a power circuit diagram of the inverter, which is used in an air conditioner for small rooms [11]. The air conditioner for small rooms is connected to each feeder with a neutral line, and their voltage rating is 105 Vrms. A three-phase variable-voltage variable-frequency inverter is used to control a three-phase AC motor, which drives the compressor in modern air conditioners. A single-phase voltage-doubler rectifier is included in the inverter circuit in Figure 3. The air conditioner for small rooms is connected to each feeder with a

neutral line, and their voltage rating is 105 Vrms. Harmonic currents are produced, and injected to the source. Single-phase diode rectifiers are also included in IH cookers and air conditioners for large rooms. Thus, these consumer electronics produce harmonic currents and inject them to the source. However, only linear loads were considered in [10], as shown in Figure 2 by Load1 and Load2. Thus, discussing the compensation performances for harmonic currents using the CDCVC-based strategy of smart charger remains an issue for further study.
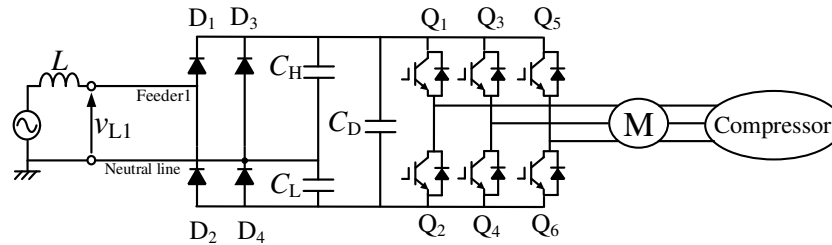

Figure 3. Single-phase voltage doubler rectifier for air conditioner [11].

This paper presents reactive, unbalanced active, and harmonic current compensation using the CDCVC-based strategy for smart charger in SPTWDFs under distorted load current conditions. The basic principle of the CDCVC-based strategy for smart chargers and the instantaneous power flowing into a smart charger are discussed in detail. This instantaneous power flowing into the smart charger shows that the previously proposed CDCVC-based strategy can compensate fundamental reactive, unbalanced active, and harmonic currents on the source side. The balanced and sinusoidal source currents with a unity power factor are achieved using only the CDCVC-based strategy, which is commonly used in active power-line conditioners. A digital computer simulation is implemented to confirm the validity and high practicability of the CDCVC-based strategy under unbalanced and distorted load current conditions. Simulation results demonstrate that sinusoidal and balanced source currents with a unity power factor are achieved on the secondary side of the PMDT during both the battery-charging and -discharging operations in EVs, compensating the reactive, unbalanced active, and harmonic currents. Simulation results also demonstrate that sinusoidal and balanced source currents with a unity power factor are achieved even though EVs are not connected to the smart charger.

2. Constant DC-Capacitor Voltage-Control-Based Strategy for Smart Chargers

Figure 4 shows a circuit diagram of the proposed smart charger, in which nonlinear loads are connected in parallel to the RL linear loads. The voltage rating of the PMDT is 6600 Vrms, 5.0 kVA, and 60 Hz on the primary side, and 105 Vrms on the secondary side. Thus, the current rating of Feeder1 and Feeder2 currents is 24 Arms. Diode rectifiers are included in modern consumer electronics. Thus, diode rectifiers in addition to linear loads are connected to each feeder with a neutral line. These diode rectifiers perform modern consumer electronics in SPTWDFs. The total harmonic distortion (THD) values were decided considering IEC61000-3-4 [12]. For the battery model, an ideal DC voltage source of 360 V_{DC} is also used. For the control algorithm of the three-leg PWM rectifier, the CDCVC-based strategy is used [10]. A proportional-integral (PI) controller was used in the CDCVC block as shown in Figure 2. In this paper, a proportional-integral-derivative (PID) controller is used to improve the response of the CDCVC-based control strategy because harmonic currents are included in addition to fundamental-reactive and -unbalanced active components of the load currents i_{L1} and i_{L2}. The difference between the PI controllers in *d-q* coordinates in Figure 2 and that in Figure 4 are explained later. The purpose of this paper is to demonstrate reactive, unbalanced active, and harmonics currents compensation of the CDCVC-based strategy of smart charger for EVs in SPTWDFs under nonlinear load conditions. Thus, ideal models for IGBTs are used.

In three-phase circuits, some control strategies for these active power-line conditioners are based on instantaneous active-reactive power theory, the so-called "*pq* theory", which was originally proposed by Akagi et al. [13–17]. The instantaneous symmetrical component theory method, the sample and hold circuit method, and the *d-q* transformation based method are also used for the calculation of the reference compensation currents [18–20]. Single-phase *pq* theory was proposed for single-phase active power line conditioners [21]. In this method, the instantaneous active-reactive power calculation block is also included. On the other hand, in Figure 4, no calculation blocks of the reactive, unbalanced active, and harmonic components of the load currents are necessary. Thus, the authors provide the simplified algorithm for smart charger. This simple control algorithm achieves balanced and sinusoidal source currents with a unity power factor. Here, the reactive, unbalanced active, and harmonic current compensation using the CDCVC-based strategy for smart charger in SPTWDFs under distorted load current conditions is discussed.
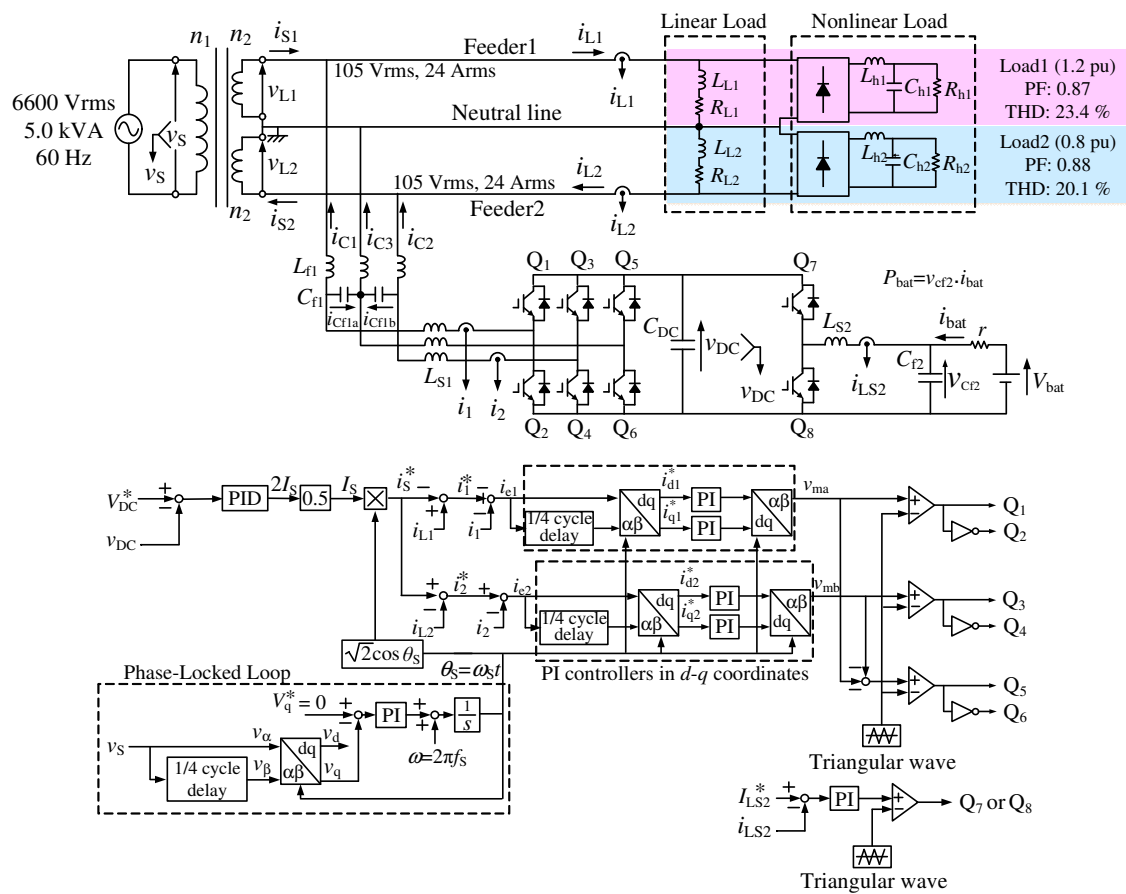

Figure 4. Circuit diagram of proposed smart charger for EVs with nonlinear loads in SPTWDFs.

Let us assume that the source voltage v_S and the secondary-side voltages v_{L1} and v_{L2} are purely sinusoidal. Then, v_S, v_{L1}, and v_{L2} are expressed as:

$$
\begin{aligned}
v_S &= \sqrt{2}V_S \cos\omega_S t, \\
v_L &= v_{L1} = v_{L2} \\
&= \sqrt{2}V_L \cos\omega_S t.
\end{aligned}
\tag{1}
$$

The load currents i_{L1} and i_{L2} in Feeder1 and Feeder2 are also expressed as:

$$
\begin{aligned}
i_{L1} &= \sqrt{2}I_{L11}\cos(\omega_S t - \phi_{L11}) + \sqrt{2}\sum_{n=2}^{\infty} I_{L1n}\cos(n\omega_S t - \phi_{L1n}), \\
i_{L2} &= \sqrt{2}I_{L21}\cos(\omega_S t - \phi_{L21}) + \sqrt{2}\sum_{n=2}^{\infty} I_{L2n}\cos(n\omega_S t - \phi_{L2n}).
\end{aligned}
\tag{2}
$$

When the reactive, unbalanced active, and harmonic components of the load currents i_{L1} and i_{L2} are compensated on the secondary side by smart charger using CDCVC-based strategy, the source currents i_{S1} and i_{S2} are balanced and sinusoidal with a unity power factor. Thus, the desired source current i_S^*, which is i_{S1} and i_{S2}, in Feeder1 and Feeder2, is expressed as:

$$
\begin{aligned}
i_S^* &= i_{S1} = i_{S2} \\
&= \sqrt{2}I_S\cos\omega_S t,
\end{aligned}
\tag{3}
$$

where I_S is the root-mean square (RMS) value of i_S^*, i_{S1}, and i_{S2}. The reference values i_{C1}^*, i_{C2}^*, and i_{C3}^* for the output currents i_{C1}, i_{C2}, and i_{C3} of the three-leg PWM rectifier are given by:

$$
\begin{aligned}
i_{C1}^* &= i_{L1} - i_{S1}, \\
i_{C2}^* &= -i_{L2} + i_{S2}, \\
i_{C3}^* &= -(i_{C1}^* + i_{C2}^*).
\end{aligned}
\tag{4}
$$

The instantaneous power p_{SC} flowing into the smart charger, which is the three-leg PWM rectifier, is given by:

$$
\begin{aligned}
p_{SC} &= -v_{L1}\cdot i_{C1} + v_{L2}\cdot i_{C2} \\
&= V_L[(-I_{L11}\cos\phi_{L11} - I_{L21}\cos\phi_{L21} + 2I_S) \\
&\quad + (-I_{L11}\cos\phi_{L11} - I_{L21}\cos\phi_{L21} + 2I_S)\cos 2\omega_S t \\
&\quad + (-I_{L11}\sin\phi_{L11} - I_{L21}\sin\phi_{L21})\sin 2\omega_S t \\
&\quad + \sum_{n=2}^{\infty}(-I_{L1n}\cos\phi_{L1n} - I_{L2n}\cos\phi_{L2n})\{\cos(n+1)\omega_S t + \cos(n-1)\omega_S t\} \\
&\quad + \sum_{n=2}^{\infty}(-I_{L1n}\sin\phi_{L1n} - I_{L2n}\sin\phi_{L2n})\{\sin(n+1)\omega_S t + \sin(n-1)\omega_S t\}].
\end{aligned}
\tag{5}
$$

If the DC-capacitor voltage v_{DC} is constant by CDCVC in Figure 4, the mean value of $\overline{p}_{SC}$ should be P_{bat} because the power charged to the battery or discharged from the battery is exchanged to the utility through the DC-capacitor C_{DC}. Thus, $\overline{p}_{SC}$ is given by:

$$
\begin{aligned}
\overline{p}_{SC} &= V_L(-I_{L11}\cos\phi_{L11} - I_{L21}\cos\phi_{L21} + 2I_S) \\
&= P_{bat}.
\end{aligned}
\tag{6}
$$

The mean value $\overline{p}_{SC}$ of instantaneous power p_{SC} flowing into the smart charger equals P_{bat} in Equation (6). Thus, the RMS value I_S of i_S^*, i_{S1}, and i_{S2} in Equation (3) is expressed as:

$$
I_S = \frac{I_{L11}\cos\phi_{L11} + I_{L21}\cos\phi_{L21}}{2} + \frac{P_{bat}}{2V_L}.
\tag{7}
$$

In the control circuit of Figure 4, the desired source current i_S^*, which are i_{S1} and i_{S2}, is generated by the output value $2I_S$ of the PID controller with $\sqrt{2}\cos\theta_s$. Thus, Equation (7) has an important implication that the mean value $\overline{p}_{SC}$ of p_{SC} is P_{bat} when the output value of the PID controller in the

CDCVC equals $2I_S$. With the CDCVC-based strategy, balanced and sinusoidal source currents with a unity power factor, which are expressed by Equation (3), are achieved on the secondary side of the PMDT charging or discharging the power P_{bat} from/to the utility grid, even though the load currents i_{L1} and i_{L2} are unbalanced and distorted. The DC-capacitor voltage v_{DC} of the three-leg PWM rectifier is detected, and then the difference ΔV_{DC} between the reference value v_{DC}^* and the detected v_{DC} is amplified by the PID controller, and then the effective value I_S of the source currents i_{S1} and i_{S2} is calculated. The reference active component i_S^* is obtained by multiplying I_S with $\sqrt{2}\cos\theta_s$, where a single-phase phase-locked loop (PLL) is used to detect the electric angle $\theta_s = \omega_s t$ of v_S [22,23]. This i_S^* is equal to that stated in Equation (3). The source voltage v_S is detected in the single-phase PLL. This v_S corresponds to the detected α-phase component v_α. The component delayed by $T_S/4$ corresponds to the β-phase component v_β. Then, v_α and v_β are transformed to v_d and v_q in *d-q* coordinates using the generated electric angle θ_s, respectively. When v_q is controlled to zero by a PI controller in *d-q* coordinates, it is possible to generate an electrical reference angle θ_s that is synchronized with v_S, which has angular frequency ω_S. Finally, by subtracting the calculated i_S^* from the detected load currents i_{L1} and i_{L2}, the reference values i_1^*, i_2^*, and i_3^* for the three-leg PWM rectifier are calculated as:

$$
\begin{aligned}
i_1^* &= i_{L1} - i_S^*, \\
i_2^* &= -i_{L2} + i_S^*, \\
i_3^* &= -(i_1^* + i_2^*).
\end{aligned}
\tag{8}
$$

It is well known that a steady-state error remains when a current controller that is a triangle intersection method based PI controller in a single-phase PWM rectifier is used. To avoid this steady-state error, an interesting current feedback control scheme in *d-q* coordinates for single-phase circuits has been proposed [24]. Figure 5 shows a block diagram of single-phase current feedback control in *d-q* coordinates, which was used in Figure 2. For i_1 in Figure 5, the reference value i_1^* is transformed into *d-q* coordinates with the $T_S/4$ delay block, which generates the β-phase component for i_1^*. The detected output current i_1 of the first leg of the three-leg PWM rectifier is also transformed into *d-q* coordinates with the $T_S/4$ delay block. The differences i_{de1} and i_{qe1} between the reference values and the detected values are calculated in *d-q* coordinates. These differences i_{de1} and i_{qe1} in *d-q* coordinates are expressed as:

$$
\begin{pmatrix} i_{d1}^* \\ i_{q1}^* \end{pmatrix} = \begin{pmatrix} \cos\theta_S & \sin\theta_S \\ -\sin\theta_S & \cos\theta_S \end{pmatrix} \begin{pmatrix} i_{1\alpha}^* \\ i_{1\beta}^* \end{pmatrix},
\tag{9}
$$

$$
\begin{pmatrix} i_{d1} \\ i_{q1} \end{pmatrix} = \begin{pmatrix} \cos\theta_S & \sin\theta_S \\ -\sin\theta_S & \cos\theta_S \end{pmatrix} \begin{pmatrix} i_{1\alpha} \\ i_{1\beta} \end{pmatrix},
\tag{10}
$$

$$
\begin{aligned}
i_{de1} &= i_{d1}^* - i_{d1} \\
&= (i_{1\alpha}^* - i_{1\alpha})\cos\theta_S + (i_{1\beta}^* - i_{1\beta})\sin\theta_S, \\
i_{qe1} &= i_{q1}^* - i_{q1} \\
&= -(i_{1\alpha}^* - i_{1\alpha})\sin\theta_S + (i_{1\beta}^* - i_{1\beta})\cos\theta_S.
\end{aligned}
\tag{11}
$$

Figure 6 shows a control circuit diagram of the single-phase current feedback in *d-q* coordinates, which is used in Figure 4. In Figure 6, for i_1, the difference i_{e1} between the reference value i_1^* and the detected value i_1 is calculated, and then transformed into *d-q* coordinates with the $T_S/4$ delay block. The differences i_{de1} and i_{qe1} are expressed as:

$$\begin{pmatrix} i_{\text{de1}} \\ i_{\text{qe1}} \end{pmatrix} = \begin{pmatrix} \cos\theta_{\text{S}} & \sin\theta_{\text{S}} \\ -\sin\theta_{\text{S}} & \cos\theta_{\text{S}} \end{pmatrix} \begin{pmatrix} i_{\text{e1}\alpha} \\ i_{\text{e1}\beta} \end{pmatrix}$$

$$= \begin{pmatrix} \cos\theta_{\text{S}} & \sin\theta_{\text{S}} \\ -\sin\theta_{\text{S}} & \cos\theta_{\text{S}} \end{pmatrix} \begin{pmatrix} i_{1\alpha}^* - i_{1\alpha} \\ i_{1\beta}^* - i_{1\beta} \end{pmatrix} \tag{12}$$

$$= \begin{pmatrix} (i_{1\alpha}^* - i_{1\alpha})\cos\theta_{\text{S}} + (i_{1\beta}^* - i_{1\beta})\sin\theta_{\text{S}} \\ -(i_{1\alpha}^* - i_{1\alpha})\sin\theta_{\text{S}} + (i_{1\beta}^* - i_{1\beta})\cos\theta_{\text{S}} \end{pmatrix}.$$

Equation (12) shows that one *d-q* transformation block is enough to achieve the current controller with a PI controller in *d-q* coordinates. Thus, two *d-q* transformation blocks are removed, as shown in Figure 4. The difference i_{de1} and i_{qe1} are amplified by PI controllers in *d-q* coordinates. The amplified differences are retransformed into *α-β* coordinates, and then the triangle intersection method is used to control the output currents i_1 and i_2.
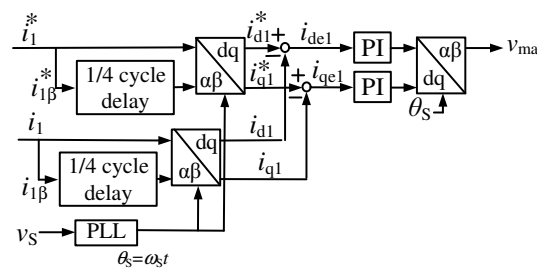

Figure 5. Control circuit diagram of single-phase current feedback control block in *d-q* coordinates in *d-q* coordinates, which was used in Figure 2.
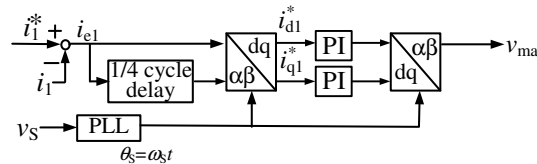

Figure 6. Control circuit diagram of single-phase current feedback control block in *d-q* coordinates in *d-q* coordinates, which was used in Figure 4.

Saitou and Shimizu [25] proposed a novel current feedback control method for single-phase circuits in *d-q* coordinates, in which a Hilbert transform is used. In their method, the Hilbert transform is implemented by numerical differentiation. This may result in instability in experimental systems. Thus, for single-phase circuits, the feedback control in *d-q* coordinates with a $T_{\text{S}}/4$ delay block is more practicable.

3. Simulation Results

The validity and high practicability of the proposed control algorithm for the proposed smart charger are confirmed by digital computer simulation using PSIM software (ver. 10.0.6.564). The unbalanced ratio between Feeder1 and Feeder2 is defined as:

$$\text{Unbalanced ratio} = \frac{S_1 - S_2}{S_{\text{A}} \times 0.5} \times 100 \ [\%], \tag{13}$$

where S_1 is the apparent power of Load1 in Feeder1, and S_2 is the apparent power of Load2 on Feeder2. S_{A} is the total apparent power, which is the sum of the apparent powers S_1 and S_2 on Feeder1 and Feeder2, respectively. According to the Japanese guidelines for domestic power consumption, the unbalanced ratio should be less than 40% for domestic power consumption [26]. Thus, Load1 of

1.2 pu is connected to Feeder1, where the power factor (PF) is 0.87, and the THD value is 23.4%. Load2 of 0.8 pu connected to Feeder2, where the PF is 0.88, and the THD value is 20.1%. Table 1 shows the circuit constants for Figure 4, which were used in the following simulation results. K_P = 0.8, T_I = 2.4 ms and T_D = 0.6 ms were used in the PID controller for CDCVC, and K_P = 0.04 and T_I = 8 ms were used in the PI controllers for current feedback control in *d-q* coordinates in Figure 4 in the following simulation results. These values of control parameters were determined with the Ziegler–Nichols ultimate sensitivity method and then improved by digital computer simulation.

Table 1. Circuit constants for Figure 4.

Item	Symbol	Value
Load1	R_{L1}	5.8 Ω
	L_{L1}	11.6 mH
(1.2 pu, power factor: 0.85, THD: 22.5%)	R_{h1}	12.5 Ω
	L_{h1}	4.7 mH
	C_{h1}	470 μF
Load2	R_{L2}	9.3 Ω
	L_{L2}	15.6 mH
(0.8 pu, power factor: 0.88, THD: 21.0%)	R_{h2}	16.8 Ω
	L_{h2}	7.4 mH
	C_{h2}	330 μF
Filter inductor	L_f	0.46 mH
Filter capacitor	C_f	10.4 μF
Switching inductor for three-leg inverter	L_{S1}	1.0 mH
DC capacitor	C_{DC}	3000 μF
DC-capacitor voltage	V_{DC}^*	385 V_{DC}
Switching inductor for DC-DC converter	L_{S2}	3.3 mH
Filter capacitor for DC-DC converter	C_{f2}	1000 μF
Battery voltage	V_{bat}	360 V_{DC}
Battery current	I_{LS2}^*	5 A_{DC}
Internal resistance of battery	r	72 mΩ
Switching frequency	f_{SW}	12 kHz
Dead time	T_d	3.5 μs

Figure 7 shows the simulation results for Figure 4, where the proposed smart charger charges the battery with constant battery current control. v_S is the source voltage, and v_{L1} and v_{L2} are the secondary-side voltage waveforms; i_{S1} and i_{S2} are the secondary-side current waveforms; i_{L1} and i_{L2} are the load-side current waveforms of the domestic consumer; i_{C1}, i_{C2}, and i_{C3} are the output current waveforms of the smart charger; v_{DC} is the DC-capacitor voltage waveform; and i_{bat} is the battery current waveform. Although the load currents i_{L1} and i_{L2} are unbalanced and distorted, the source currents i_{S1} and i_{S2} are balanced and sinusoidal with a unity power factor. The THD values of i_{S1} and i_2 are 4.2% and 3.4% respectively, under the steady state, and the voltage ripple of v_{DC} is 1.35%. Figure 8 shows the simulation results for Figure 4, where the proposed smart charger discharges the battery with constant battery current control. Although the load currents i_{L1} and i_{L2} are unbalanced and distorted, the source currents i_{S1} and i_{S2} are balanced with a unity power factor. The THD values of i_{S1} and i_{S2} are 10.8% and 7.7%, respectively, under the steady state, and the voltage ripple of v_{DC} is 1.30%. Simulation results have demonstrated that sinusoidal and balanced source currents with a unity power factor are achieved on the secondary side of the PMDT during the battery-charging and -discharging operations in EVs, thereby compensating the reactive, unbalanced active, and harmonic currents. Simulation results also have demonstrated that sinusoidal and balanced source currents with a unity power factor are achieved even though EVs are not connected to the smart charger. Thus, the proposed smart charger can solve the power quality problems and reduce losses in the PMDTs. Figure 9 shows the simulation results for Figure 4, where an EV is not connected to the proposed smart charger. Thus, the smart charger performs as an active power-line conditioner for the domestic

consumer. Although the load currents i_{L1} and i_{L2} are unbalanced and distorted, the source currents i_{S1} and i_{S2} are balanced with a unity power factor. The THD values of i_{S1} and i_{S2} are 4.6% and 3.8% respectively, under the steady state, and the voltage ripple of v_{DC} is 1.19%.

The required capacity of the three-leg PWM rectifier, which performs as a smart charger, is now discussed. A definition of apparent power is generally used to calculate the required capacity of the PWM rectifier. The third leg of the PWM rectifier, which is connected to the neutral line, is grounded. The typically used definition of apparent power is not applicable to the three-leg PWM rectifier. In [27], the authors have defined a current capacity A_C for the smart charger with a PWM rectifier in single-phase three-wire distribution feeders. A_C is given as:

$$A_C \quad = \quad \frac{\sum_{n=1}^{3} I_{Cn}}{2 I_A} \quad \text{pu,} \tag{14}$$

where I_A is the rating of Feeder1 and Feeder2 currents. The rating of the PMDT is 6600 Vrms, 5 kVA, and 60 Hz on the primary side, and 105 Vrms on the secondary side. Thus, I_A is 24 Arms. From the simulation results in Figure 7, A_C is 0.91 pu.

Table 2 shows relationships between the current capacity A_C and load conditions. The current capacity A_C with the larger unbalanced ratio, which is defined by Equation (14), is larger with the larger load conditions. As mentioned above, the maximum-acceptable unbalanced ratio is 40% according to Japanese guidelines for domestic power use [26]. Thus, the current capacity A_C of 0.91, which is calculated from the simulation results of Figure 7, gives the maximum current capacity of the three-leg PWM rectifier, which performs as a smart charger. The THD values of the source currents i_{S1} and i_{S2}, in Figures 7–9, satisfy the regulations [12]. Experimental verifications for Figure 4 are an important issue. Thus, experimental results will be reported in another article.

Table 2. Relationships between current capacity A_C and load conditions.

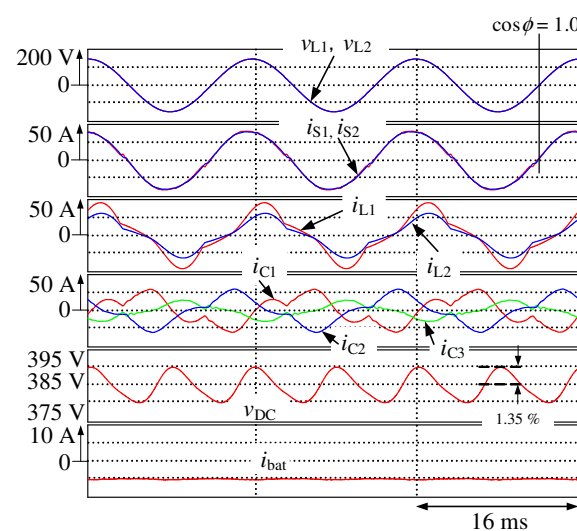| Unbalanced Ratio	Load Conditions		THD Values				Current Capacity A_C pu
	Load1	Load2	i_{L2}	i_{L2}	i_{S1}	i_{S2}	
40%	1.2 pu	0.8 pu	23.6%	22.9%	4.2%	3.4%	0.91
	1.0 pu	0.67 pu	23.8%	23.0%	4.3%	3.4%	0.83
	0.8 pu	0.53 pu	25.0%	23.9%	4.3%	3.4%	0.76
20%	1.2 pu	1.0 pu	22.6%	20.0%	3.8%	5.0%	0.85
	1.0 pu	0.67 pu	23.6%	20.4%	3.7%	3.6%	0.78
	0.8 pu	0.53 pu	25.0%	36.3%	2.5%	2.2%	0.72

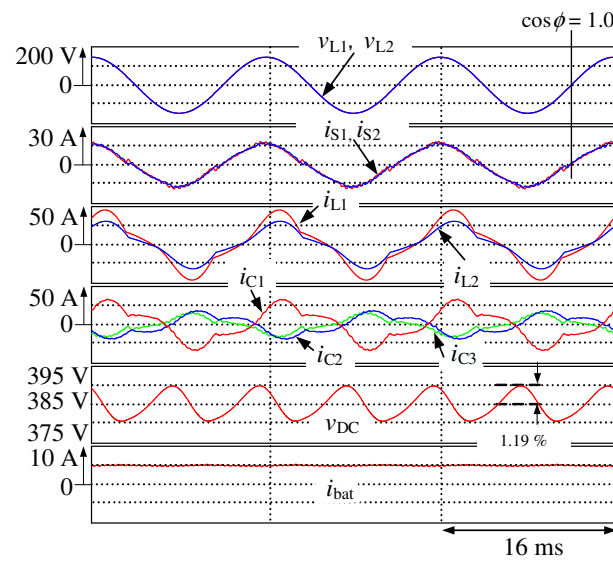**Figure 7.** Simulation results for Figure 4 during battery-charging operation.

Figure 8. Simulation results for Figure 4 during battery-discharging operation.
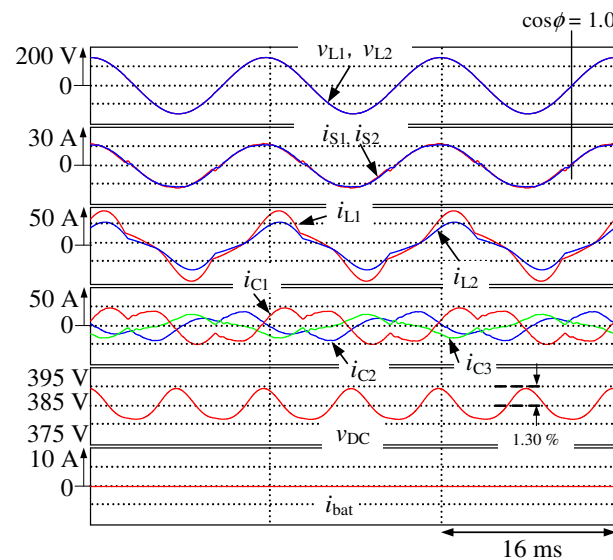

Figure 9. Simulation results for Figure 4 without battery, where smart charger performs active power-line conditioner.

4. Conclusions

This paper has presented reactive, unbalanced active, and harmonic current compensation using the CDCVC-based strategy of the smart charger in SPTWDFs under unbalanced and distorted load current conditions. The instantaneous power flowing into the smart charger has been discussed in detail. This instantaneous power flowing into the smart charger shows that the previously proposed CDCVC-based strategy can compensate for reactive, unbalanced active, and harmonic currents on the source side. This results in the balanced and sinusoidal source currents with a unity power factor using only the CDCVC-based strategy, which is commonly used in active power-line conditioners. Thus, the previously proposed CDCVC-based strategy is applicable under unbalanced and distorted load conditions. A digital computer simulation has been implemented to confirm the validity and practicability of the previously proposed CDCVC-based strategy under unbalanced and distorted load current conditions using PSIM software. Simulation results have demonstrated that sinusoidal and balanced source currents with a unity power factor are achieved on the secondary side of the

PMDT during the battery-charging and discharging operations in EVs, thereby compensating for the reactive, unbalanced active, and harmonic currents. Simulation results also have demonstrated that sinusoidal and balanced source currents with a unity power factor are achieved even though EVs are not connected to the smart charger.

Author Contributions: Fuka Ikeda significantly contributed to demonstrate the basic principle of the constant dc-capacitor voltage-control-based strategy and contributed to the design of the proposed control strategy and the implementation of the digital computer simulation. Toshihiko Tanaka proposed the control strategy and helped with the writing of this paper. Hiroaki Yamada and Masayuki Okamoto were responsible for guidance and key suggestions.

Conflicts of Interest: The authors declare no conflict of interest.

References

1. Available online: http://www.meti.go.jp/committee/summary/0004668/pdf/0120300.pdf (accessed on 10 January 2012).

2. Mitani, Y. Method and System for Leveling Power Load. Japan Patent Office 4862 153 (P4 862 153), 25 January 2012.

3. Available online: http://www.nissan-global/com/JP/NEWS/ (accessed on 10 January 2012).

4. Yilmaz, M.; Krein, P.T. Review of benefits and challenges of Vehicle-to-Grid technology. In Proceedings of the IEEE Energy Conversion Congress and Exposition (ECCE), Raleigh, NC, USA, 15–20 September 2012; pp. 3082–3089.

5. Cvetkovic, I.; Thacker, T.; Dong, D.; Francis, G.; Podosinov, V.; Boroyevich, D.; Wang, F. ; Burgos, R.; Skutt, G.; Lesko, J. Future home uninterruptible renewable energy system with Vehicle-to-Grid technology. In Proceedings of the IEEE Energy Conversion Congress and Exposition (ECCE), San Jose, CA, USA, 20–24 September 2009; pp. 2675–2681.

6. Gurkaynak, Y.; Khaligh, A. Control and power management of a grid connected residential photovoltaic system with plug-in hybrid electric vehicle (PHEV) load. In Proceedings of the IEEE Energy Conversion Congress and Exposition (ECCE), Washington, DC, USA, 15–19 February 2009; pp. 2086–2091.

7. Monteiro, V.; Pinto, J.G.; Exposto, B.; Goncalves, H.; Ferreira, J.C.; Couto, C.; Afonso, J.L. Assessment of a battery charger for electric vehicles with reactive power control. In Proceedings of the Industrial Electronics Conference (IECON), Montreal, QC, Canada, 25–28 October 2012; pp. 5124–5129.

8. Kisacikoglu, M.C.; Ozpineci, B.; Tolbert, L.M. Examination of a PHEV bidirectional charger system for V2G reactive power compensation. In Proceedings of the IEEE Applied Power Electronics Conference and Exposition, Palm Springs, CA, USA, 21–25 February 2010; pp. 458–465.

9. Kisacikoglu, M.C.; Ozpineci, B.; Tolbert, L.M. Reactive power operation analysis of a single-phase EV/PHEV bidirectional battery charger. In Proceedings of the 8th International Conference Power Electronic-ECCE Asia, Jeju, Korea, 30 May–3 June 2011; pp. 585–591.

10. Tanaka, T.; Sekiya, T.; Tanaka, H.; Hiraki, E.; Okamoto, M. Smart charger for electric vehicles with power quality compensator on single-phase three-wire distribution feeders. *IEEE Trans. Ind. Appl.* **2013**, *49*, 2628–2635.

11. Uesugi, M.; Kanazawa, H.; Hiruma, A.; Miyazaki, H.; Kanbe, T. Single-phase twice voltage PFC converter for air conditioner. *IEEJ Trans. Ind. Appl.* **1999**, *119*, 592–598.

12. IEC61000-3-4. *Electromagnetic Compatibility (EMC)—Part 3-4: Limits—Limitation of Emission of Harmonic Currents in Low-Voltage Power Supply Systems for Equipment with Rated Current Greater Than 16 A*; International Electrotechnical Commission: Geneva, Switzerland, 1998.

13. Akagi, H.; Kanazawa, Y.; Nabae, A. Instantaneous reactive power compensators comprising switching devices without energy storage components. *IEEE Trans. Ind. Appl.* **1984**, *IA-20*, 625–630.

14. Nava-Segura, A.; Mino-Aguilar, G. Four-branches-inverter-based-active-filter for unbalanced 3-phase 4-wires electrical distribution systems. In Proceedings of the IEEE Industrial Applied Conference, Roma, Italy, 8–12 October 2000; Volume 4, pp. 2503–2508.

15. Peng, F.Z.; Ott, G.W.; Adams, D.J. Harmonic and reactive power compensation based on the generalized instantaneous reactive power theory for the three-phase four-wire systems. *IEEE Trans. Power Electron.* **1998**, *13*, 1174–1181.

16. Singh, B.N.; Rast, P. A new topology of active filter to correct power-factor, compensate harmonics, reactive power and unbalance of three-phase four-wire loads. In Proceedings of the IEEE Applied Power Electronics and Exposition, Miami Beach, FL, USA, 9–13 February 2003; Volume 1, pp. 141–147.

17. Adya, A.; Mittal, A.P.; Gupta, J.R.P. Modeling and control of DSTATCOM for three-phase, four-wire distribution systems. In Proceedings of the Conference Record of IEEE-IAS Annual Meeting, Kowloon, Hong Kong, China, 2–6 October 2005; Volume 4, pp. 2428–2434.

18. Geddada, N.; Karanki, S.B.; Mishra, M.K.; Kumar, B.K. Modified four leg DSTATCOM topology for compensation of unbalanced and nonlinear loads in three phase four wire system. In Proceedings of the 14th European Conference on Power Electronics and Applications (EPE 2011), Birmigham, UK, 30 August–1 September 2011.

19. Dixon, J.W.; Garcia, J.J.; Moran, L. Control system for three-phase active power filter which simultaneously compensates power factor and unbalanced loads. *IEEE Trans. Ind. Electron.* **1995**, *42*, 636–641.

20. Abllan, A.; Garcera, G.; Pascual, M.; Figueres, E. A new current controller applied to four-branch inverter shunt active filters with UPF control method. In Proceedings of the IEEE Power Electronics Specialist Conference (PESC), Vancouver, BC, Canada, 17–21 June 2001; Volume 3, pp. 1402–1407.

21. Tarafdar Haque, M. Single-phase pq theory for active filters. In Proceedings of the IEEE TRNCON, Beijing, China, 28–31 October 2002; Volume 3, pp. 1941–1944.

22. Arruda, L.N.; Silva, S.M.; Filho, B.J.C. PLL structures for utility connected systems. In Proceedings of the Conference Record of IEEE-IAS Annual Meeting, Chicago, IL, USA, 30 September–4 October 2001; pp. 2655–2660.

23. Silva, S.M.; Lopes, B.M.; Filho, B.J.C.; Campana, R.P.; Boaventura, W.C. Performance evaluation of PLL algorithms for single-phase grid-connected systems. In Proceedings of the Conference Record of IEEE-IAS Annual Meeting, Seattle, WA, USA, 3–7 October 2004; pp. 2259–2263.

24. Zhang, R.S.; Clifton, P. Control of Single-Phase Power Converter in *d-q* Coordinates. U.S. Patent 6,621,252, 16 September 2003.

25. Saitou, M.; Shimizu, T. A control method of single phase power active filter on *d-q* coordinate with hilbert transformer. *IEEJ Trans. IA* **2002**, *122*, 193–194. (In Japanese)

26. Japan Electric Association. *Indoor Wiring Guidelines*; JESC E0005; Japan Electric Association: Chiyoda-ku, Japan, 2005; p. 32. (In Japanese)

27. Tanaka, H.; Wakimoto, T.; Tanaka, T.; Okamoto, M.; Hiraki, E. Reducing capacity of smart charger for electric vehicles on single-phase three-wire distribution feeders with reactive power control. *IEEJ J. Ind. Appl.* **2014**, *3*, 437–445.